Senescence driven solubilization of biomass is the main source of kelp-derived dissolved organic carbon to the coastal ocean

Chance J. English[1*], *Tom W. Bell*[2], *Keri Opalk*[1], *Dave A. Siegel*[3], *Craig A. Carlson*[1]

1. Marine Science Institute/Department of Ecology, Evolution and Marine Biology, University of California Santa Barbara, CA, USA

2. Department of Applied Ocean Physics and Engineering, Woods Hole Oceanographic Institution, Woods Hole, MA 02543

3. Earth Research Institute/Department of Geography, University of California, Santa Barbara, CA 93106

* Corresponding author: Chance J. English

Email: cje@ucsb.edu

(951) 286-8416

Key Words: macroalgae, dissolved organic carbon, senescence, carbohydrates, carbon dioxide removal, carbon sequestration

Author Contribution Statement

CJE and CAC conceptualized the research. CJE collected material for and ran the incubations. CJE, TWB, and KO collected data and performed laboratory measurements. CJE, TWB, KO, DAS and CAC contributed to interpreting the results and writing/editing the manuscript. CAC, TWB, and DAS acquired funding for the research.

Abstract

Kelp forests form some of the most productive areas on earth and are proposed to sequester carbon in the ocean, largely in the form of released dissolved organic carbon (DOC). Here we investigate the role of environmental, seasonal and age-related physiological gradients on the partitioning of net primary production (NPP) into DOC by the canopy forming giant kelp (*Macrocystis pyrifera*). Rates of DOC production were strongly influenced by an age-related decline in physiological condition (i.e. senescence). During the mature stage of giant kelp development, DOC production was a small and constant fraction of NPP regardless of tissue nitrogen content or light intensity. When giant kelp entered its senescent phase, DOC production increased substantially and was uncoupled from NPP and light intensity. Compositional analysis of giant kelp-derived DOC showed that elevated DOC production during senescence was due to the solubilization of biomass carbon, rather than by direct exudation. We coupled our incubation and physiological experiments to a novel satellite-derived 20-year time series of giant kelp canopy biomass and physiology. Annual DOC production by giant kelp varied due to differences in standing biomass between years, but on average, 74% of the annual DOC production by giant kelp was due to senescence. This study suggests DOC may be a more important fate of macroalgal NPP than previously recognized.

Introduction

Dissolved organic carbon (DOC) serves important ecological and biogeochemical roles in the ocean, including the structuring of microbial communities and the sequestration of carbon[1]. While there are many sources of DOC to the ocean, including phytoplankton exudation and river discharge, little is known about the contribution from coastal vegetated ecosystems (CVEs),

including those dominated by mangroves, seagrasses, and macroalgae. In recent years, there have been efforts to constrain the flux of carbon from CVEs, aiming to integrate these ecosystems into estimates of marine carbon sequestration (i.e. blue carbon) [2–4]. These efforts are critical, as there is a growing movement to restore, conserve, and expand CVEs to enhance their ecosystem capacity as carbon sinks and sequester atmospheric CO_2 [5–7].

Marine macroalgae form some of the most productive areas on earth and fix an estimated 1-3% of marine net primary production (NPP) [8,9]. Unlike other CVEs, macroalgae do not store carbon in the benthos, and most of their fixed carbon is exported from their habitats as dissolved organic carbon or particulate detritus [10–12]. A synthesis of macroalgal NPP and export pathways found that naturally occurring macroalgal systems potentially sequester about 173 (range = 61-268) Tg C yr^{-1}, of which 70% is in the form of DOC [12]. However, uncertainties in macroalgal biomass, NPP, and assumptions of macroalgal DOC production, remineralization rates, and export efficiencies call these estimates into question [13–15]. A major uncertainty in the production and fate of macroalgal NPP is the fraction that is partitioned into DOC, which is reported to range from <1 to 76% [11,13,16–22]; therefore understanding the controls on DOC release rates by macroalgae is critical to their integration into blue carbon budgets. Environmental factors such as light intensity and nutrient availability are considered key regulators of DOC release by aquatic primary producers (see review of the overflow hypothesis[23] in ref. 1). However, studies of macroalgae DOC release that only consider these two factors have reported conflicting results [11,20,22,24], suggesting that factors other than extrinsic ones may regulate macroalgal DOC production. Unlike extrinsic factors, such as light and nutrient availability, little attention has been given to the intrinsic factors associated with macroalgae physiology and life cycles, such as senescence. Knowledge about physiology is critical as primary producers can undergo rapid

physiological changes that modulate their response to environmental factors [25,26]. Therefore, we hypothesized that consideration of intrinsic (age, senescence) as well as extrinsic (light and nutrients) factors must be considered to improve our understanding of DOC production by macroalgae.

Macrocystis pyrifera, hereafter referred to as giant kelp, is a globally distributed species that forms canopies visible from space [27]. Single "plants" consist of up to hundreds of fronds, each with an average lifespan of about 100-120 days [28]. Each frond consists of a single stipe with leaf-like blades that photosynthesize and take up nutrients from the surrounding seawater. Growth occurs year-round through the initiation of new fronds, and tissue physiology, including its carbon to nitrogen ratio and chlorophyll *a* content are influenced by the availability of light and nutrients [29]. As fronds grow, blades emerge from the growing tip, creating a gradient in blade age along the frond. This pattern of growth results in large age-distributions of giant kelp biomass both within and between individual plants [30]. As a consequence of age, and regardless of ambient environmental conditions, giant kelp undergoes progressive senescence, a rapid decline in physiological condition resulting in the loss of biomass without external forces such as waves or herbivory [28,30]. While it has been established that senescence increases the rate of particulate detritus shed by giant kelp [31], the impact of senescence on DOC production rates in giant kelp has not been considered.

To address the role of intrinsic and extrinsic factors on DOC production by giant kelp, we performed incubations of giant kelp blades sampled from tagged frond cohorts over several months in the summer and spring periods in the Santa Barbara Channel, CA. We demonstrate that consideration of senescence explains large variability in DOC production by giant kelp. Further, we demonstrate the senescence-driven DOC production is likely due to the

solubilization of existing biomass carbon, rather than by direct exudation. We applied our findings to a novel, large-scale time-series data set that monitored variability of giant kelp canopy biomass and physiology. Our results demonstrate that senescence-driven solubilization drives most of the DOC released from giant kelp to the coastal ocean.

Methods

Kelp collection and incubations

Giant kelp blades were collected from Mohawk Reef (34.3941° N, 119.7296° W) in Santa Barbara, California, between August 2023 and June 2024. At each sampling event (n = 9), six whole blades were clipped between the pneumatocyst and stipe and transported back to a nearshore laboratory in surface seawater and placed in 10 L acrylic incubation tanks filled with 0.2 µm filtered seawater collected the day before. Blades were allowed 30 minutes to acclimate to the incubation chambers to prevent sampling of exudation driven by handling. Incubation tanks were outfitted with magnetic stir bars to maintain circulation within the chambers. The six collected kelp blades were incubated a three light levels between 0-1517 µmol m^{-2} s^{-1} for 2-3 hours.

Environmental & Physiological Variables

Incubation light levels were controlled using a dimmable LED light source (VIPARSPECTRA XS4000, Richmond, CA USA) and measured with a photosynthetically active radiation (PAR) meter (Phantom PHOTOBIO, Chico, CA USA). Physiological measurements such as age, tissue stoichiometry and pigment concentrations were determined by previously established methods [29,32,33]. Age cohorts of giant kelp were established in August

2023 (summer cohort) and April 2024 (spring cohort). Tissue age was measured by tagging up to 100-200 fronds 2m back from the growing tip (blade age ~ 14 days; based on frond elongation rates of ~ 14 cm d^{-1} [34,35]). Two days after tagging the cohorts, a single blade was sampled at the tag site from six random fronds every 2-3 weeks for up to 78 days. Following incubations, tissue was rinsed with 10% HCl followed by deionized water to remove any $CaCO_3$ from epibionts and dried at 60 °C for three days. Dried tissue was weighed, ground to a fine powder, and analyzed for carbon and nitrogen content using an CE-440 CHN/O/S elemental analyzer (Exeter Analytical, Exeter, UK). Chlorophyll *a* (Chl*a*) concentrations were measured from a 0.8 cm^2 disk excised from the tissue before rinsing and drying. Disks were weighed and sequentially extracted in 4 ml of dimethyl sulfoxide and 5 ml of acetone, methanol, and ultrapure water (3:1:1). The absorbance of the extracts was measured from 350 nm to 800 nm (Shimadzu UV 2401PC, Tokyo, Japan) [29,36]. Chl*a* concentration was calculated from absorption spectra following Seely et al., (1972). The physiological parameter, Chl:C was measured by dividing the mass of Chl*a* by the dry mass of carbon for each excised disk.

Net Primary Production

NPP was measured as changes in dissolved inorganic carbon (DIC) in the incubation seawater. Samples were collected by overflowing a 125 ml glass serum bottle with incubation seawater and preserved with 120µl of saturated $HgCl_2$. DIC samples were analyzed by acidifying the sample with 10% H_3PO_4 and sparging with N_2 for 220 seconds. The resulting CO_2 in the gas stream was measured via an automated, non-dispersive infrared inorganic carbon analyzer with an AIRICA TCO_2 analyzer (MARIANDA, Kiel, Germany) [37]. The pCO_2 peak area was converted to µmol C L^{-1} using a coefficient calculated from a certified reference material (CRM

142 Batch #206 & #216; Dickson Lab, San Diego, CA USA). CRMs were run every 12 samples to
143 check for analytical stability throughout a given run. The average standard deviation from three
144 CRM technical replicates across each run was 2.9 ± 1.9 µmol C L^{-1}. Rates of NPP were
145 calculated as follows:

146 $$\text{NPP } (\mu\text{mol C } g_{DW}\ hr^{-1}) = \frac{[DIC]_0 - [DIC]_t * V}{T * m} \quad (1)$$

147 where $[DIC]_0$ and $[DIC]_t$ are the DIC concentrations (µmol C L^{-1}) at the beginning and end of
148 each incubation, respectively. V is the volume of seawater during the incubation, T is the
149 incubation time, and m is the tissue dry weight.
150
151 *DOC Analyses*
152 DOC analysis was carried out according to Halewood et al., 2022[38]. Briefly, duplicate
153 samples for DOC were collected from the beginning and end of each incubation, filtered through
154 pre-combusted 25 mm GF-75 (nominal pore size of 0.3 µm) into pre-combusted 40 mL EPA
155 vials with PTFE lined caps, and acidified to pH ~2 with 4N HCl. DOC concentrations were
156 quantified by the high-temperature combustion method using a TOC-V or TOC-L (Shimadzu,
157 Tokyo, Japan) using a four-point glucose standard curve. Each run was also referenced against
158 surface and deep seawater collected from near the Bermuda Atlantic Time Series study site and
159 calibrated against consensus reference material (Hansell Deep Sea Reference Batch #21,
160 Lot#04–21, Miami, FL USA) run every 6–8 samples. The precision for the analytical runs had a
161 coefficient of variation of duplicate samples < 2% or ± 0.6 µM C for this study. DOC exudation
162 rates (DOC_{ex}) were calculated as follows:

163 $$DOC_{ex}\ (\mu\text{mol C } g_{DW}\ hr^{-1}) = \frac{[DOC]_t - [DOC]_0 * V}{T * m} \quad (2)$$

where $[DOC]_t$ and $[DOC]_0$ are the DOC concentrations in μmol C L^{-1} at the end and beginning of each incubation, respectively. V is the volume of seawater during the incubation, T is the incubation time, and m is the tissue dry weight.

Giant Kelp Exudate Composition

Kelp-derived DOC was analyzed for its carbohydrate content and specific sugar monomer composition. The sugar content of the exudates was measured using high-performance anion exchange chromatography with pulsed amperometric detection (HPAEC-PAD), following dialysis and eluent gradient protocols specified in Engel and Händel (2011)[39]. Briefly, samples were dialyzed using Spectra/Por 7 tubing (1000 Da) against ultrapure water, then hydrolyzed for 20 hours at 100°C in 0.4 M HCl and neutralized under N_2. Samples were run on a DIONEX ICS5000+ (Thermo Fisher Scientific) and separated using a Carbopac PA10 column (4x250mm) with a Carbopac PA10 guard column (4x50mm). Neutral and amino sugars were eluted isocratically with 18mM NaOH and followed by 100mM NaOH/200mM Na-Acetate to elute acidic sugars. The system was calibrated using a standard sugar mix containing fucose, rhamnose, arabinose, galactosamine, glucosamine, galactose, glucose, mannose+xylose, galacturonic acid, glucuronic acid and mannuronic acid (Sigma-Aldrich ≥99%). Linearity of the calibration curves was observed for concentrations ranging from 10 nM-1μM. Due to leaching of glucose and mannose+xylose rich carbohydrates from the Spectra/Por 7 dialysis tubing, these sugars were removed from further analysis.

Estimates of regional giant kelp canopy biomass, age and DOC production

To extrapolate our measured giant kelp DOC_{ex} rates to regional scales, we determined giant kelp canopy biomass and age distribution using Landsat 7, 8, and 9 multispectral imagery focusing on the central and southern California coastline where giant kelp dominates. Between the years 2001-2023, we created a spatial time-series of giant kelp canopy biomass estimates at the native Landsat 30m pixel resolution [27]. Biomass was then interpolated for each pixel to a monthly time scale using a 'makima' interpolation with the interp1 function in Matlab. There was an average of 23.3 (standard deviation = 3.6) cloud-free views per year for each pixel for this region for the years 2001 and 2023, allowing for this monthly time-series to be created. From this monthly timeseries, we resampled to a daily resolution and found the difference in kelp canopy biomass between each date using the diff function in Matlab. Positive changes in kelp biomass were then tracked where the first appearance of biomass increased, given an age of one day, and accounted for until the age of 120 days[28], when canopy biomass was assumed to be completely senesced and lost. By completing this step for each pixel timeseries, we estimated the age of the canopy biomass for each month of the time-series across the study domain. We then multiplied these fractions by the monthly satellite-derived biomass yielding the wet weight in kg of biomass for all ages for each month and pixel across the central and southern California coastline. Kelp canopy biomass was converted from wet weight to dry weight using the average dry weight:wet weight ratio of 0.12 measured in our incubations.

Using our incubation-derived, dry mass normalized DOC production rates (eq. 2) we estimated annual DOC production along the California coastline. We calculated daily DOC_{ex} for mature kelp assuming a 12-hour light/dark cycle and the mass normalized DOC_{ex} rates measured in the dark (PAR = 0 μmol m^{-2} s^{-1}) and light saturating (PAR > 300 μmol m^{-2} s^{-1}) incubations. We then calculated daily DOC release from senescent kelp using the estimated amount of

senescent biomass and our measured senescent DOC_{ex} rates. To account for the uncertainty in DOC_{ex} rates observed in our incubations, we calculated a probability distribution for each of the parameters from our laboratory incubations. We performed a bootstrap analysis with 100,000 simulations to derive a median and 95% confidence interval for DOC_{ex} rates for mature kelp in the dark and light-saturating conditions as well as for senescent kelp. Daily rates were then used to derive an annual estimate of giant kelp DOC production along the central and southern California coastline between 2001 and 2023.

Statistical Analysis

To compare means between two independent variables that were approximately normal but did not have equal variances, we used Welch's t-test. To compare means between two independent variables that were not normal we used the non-parametric Wilcoxon rank sum test. Model II linear correlation analysis was used to compare the relationships when both variables were assumed to have equal random error (i.e. DOC_{ex}, NPP). Ordinary least squares (OLS) regression was used to compare the relationship between variables when one variable was assumed not to have random error (i.e. light, age). To visualize how giant kelp-derived exudate composition changed between mature and senescent blades, we conducted a principal component analysis of scaled molar percentages of individual sugars. Differences in the composition of exudates between maturity and senescence was assessed using permutational multivariate analysis of variances (PERMANOVA).

Results

Age and seasonal-driven changes in kelp physiology and NPP

To better understand how intrinsic and extrinsic factors influence the partitioning of NPP into DOC production by giant kelp, we measured both from kelp sampled during nutrient deplete (summer) and replete (spring) periods over blade ages of 16-78 days (Supplemental Table 1). The ages of sampled blades in both seasons covered the periods from early to late maturity (16-43 days) through early to late senescence (58-78 days). We observed large, rapid changes in kelp physiological condition, as measured by its Chl:C content, after 50 days of age in both seasons and hereby refer to kelp tissue younger or older than 50 days as "mature" or "senescent", respectively (Figure 1a). Mature summertime giant kelp C:N was on average 29.6 ± 3.6, three times larger than average mature springtime C:N (mean ± 1SD = 10.1 ± 0.7). In both the summer and spring cohorts, there was an increase in average tissue C:N with age (Supplemental Table 1). Mature spring kelp had a significantly higher Chl:C content (Welch's t-test, $t = 5.8$, $df = 13.6$, $p < 0.001$) and significantly lower C:N (Welch's t-test, $t = -22.5$, $df = 19.0$, $p < 0.001$) than mature summer kelp. Both cohort's Chl:C content had a non-linear and rapid decline after 50 days of age (Figure 1a).

Across all incubations, NPP rates ranged from -30.3 to 264.9 μmol C g_{DW}^{-1} hr^{-1} (Figure 1b). As expected, rates of NPP displayed a non-linear response to light, increasing rapidly with exposure to low light levels and saturating at PAR values > 300 μmol m^{-2} s^{-1} (Supplemental Figure 1a). In both seasons, there was a significant linear decrease in maximum photosynthetic rates with age (Ordinary Least Squares (OLS) regression, Summer: $R^2 = 0.85$, $p < 0.001$, $n = 30$; Spring: $R^2 = 0.44$ $p < 0.001$, $n = 24$), although the spring cohort had a slower rate of decline with age than the summer cohort (Supplemental Figure 1b). Negative photosynthetic rates reported are apparent respiration rates when PAR was equal to zero.

Giant kelp DOC release rates

Rates of DOC release (DOC_{ex}) by giant kelp blades were influenced by both extrinsic and age-driven intrinsic processes, namely NPP, light, and senescence, respectively (Figure 2). DOC_{ex} ranged from -1.2 – 65.3 μmol C g_{DW}^{-1} hr^{-1} across all incubations (Supplemental Table 1). Two data points were excluded from our analysis due to accidental physical damage to the kelp tissue by the incubator stir bars resulting in artificially high DOC_{ex}. These data points are included, and their exclusion is discussed in Supplemental Figure 2.

Within each season, there was a significant increase in DOC_{ex} between mature and senescent kelp (Wilcoxon Test, Summer: W = 189.5, p = $8.7e^{-10}$; Spring: W = 275, p = $2.7e^{-5}$). In mature kelp blade incubations, there was a significant linear correlation between rates of NPP and DOC_{ex} (Figure 2a; Model II; R^2 = 0.27; p = $1.81e^{-7}$, n = 88). Percent extracellular release (PER) was calculated as DOC_{ex} /NPP * 100% for incubations where NPP > 0. In mature kelp incubations, average PER (±1SD) was 2.7 (±1.2) % and 2.3 (±2.2) % of NPP, in the spring and summer, respectively. As a test of the overflow hypothesis[23], we compared the relationship between PER and tissue C:N and light intensity. Although we found a significant negative relationship between PER and tissue C:N, opposite to the predictions of the overflow hypothesis, it was a poor predictor variable (Supplemental Figure 3a; Model II, p = 0.037, R^2 = 0.08, n = 73). For example, across a gradient of tissue C:N from 10 to 40 it would only predict a change in PER from 3.0% to 1.6%, a range within one standard deviation of the average PER in both seasons. In addition, PER showed no significant variability with irradiance level (Supplemental Figure 3b, OLS, p = 0.48, R^2 = -0.006, n = 73). In mature kelp incubations, DOC_{ex} continued in the dark (PAR = 0 μmol m^{-2} s^{-1}) at an average (±1 SD) rate of 0.9 (±1.0) μmol C g_{DW}^{-1} hr^{-1}, approximately three times lower than rates in light saturating conditions (306 - 1517 μmol m^{-2} s^{-}

278 ^{1}), which averaged (± 1SD) 3.3 (±2.0) µmol C g_{DW}^{-1} hr^{-1}. DOC_{ex} by mature kelp was also
279 positively, correlated with light intensity (OLS; $R^2 = 0.14$, $p = 2.56e^{-6}$, n = 88), but light intensity
280 was a weaker predictor variable than the rate of NPP.
281 As blades entered the senescent phase, DOC_{ex} became uncoupled from NPP (Figure 2b)
282 and was not correlated with light intensity (OLS, $R^2 = 0.00$, p = 0.54, n = 70). This decoupling
283 of DOC_{ex} and NPP with age occurred in both the spring and summer cohorts following the onset
284 of senescence (Figure 2b, Supplemental Table 1). Notably, DOC_{ex} in the senescent phase often
285 equaled or exceeded simultaneous rates of NPP. These elevated rates continued in the dark,
286 suggesting a continuous, large release of DOC by senescent blades, but were highly variable
287 across all senescent blade incubations (mean ± 1SD = 14.0 ± 14.1 µmol C g_{DW}^{-1} hr^{-1}). This large
288 variability in senescent kelp DOC_{ex} is, in part due to the progressive senescence of giant kelp
289 blades as they aged beyond 50 days. We observed that senescent kelp DOC_{ex} rates increased as
290 physiological conditions, measured as chlorophyll *a* content normalized to the maximum
291 observed in each seasonal cohort, declined (Supplemental Figure 4; Model II, $R^2 = 0.35$, $p <$
292 0.001, n = 70).
293
294 *DOC Composition*
295 The total carbohydrates fraction released by giant kelp blades remained a relatively
296 constant proportion of the released DOC in all incubations, averaging 10.3 ± 4.9%, however the
297 relative contribution of any given specific hydrolyzable sugar was more variable. For example,
298 we observed a significant difference in the mole% of sugars in the kelp exudates between the
299 mature and senescent stages (Figure 3a, PERMANOVA; p = 0.001, $R^2 = 0.14$, n = 42). These
300 differences were mostly driven by the mole% of fucose and mannuronic acid (Man-URA) which

constituted an average of 47% and 34%, respectively of the sugars exuded in the mature and senescent phases, respectively (Figure 3c & 3d). On average fucose comprised 47% and 32% of the carbohydrate monomers from mature and senescent kelp exudates, respectively. Man-URA had the largest change in mole% of all sugars between the mature and senescent phase, increasing 7-fold from an average mole% of 5 to 34%, respectively (Figure 3c & 3d).

Regional estimates of giant kelp canopy biomass, physiology, and senescence-driven DOC production

Monthly changes in canopy biomass across central and Southern California between 2001 – 2023 were assessed using Landsat multispectral imagery. At this scale, giant kelp canopy biomass showed a regular pattern of seasonal growth in the spring, resulting in a peak in biomass in the summer (Figure 4a). The total giant kelp biomass showed large intra- and interannual variability, ranging from 2 – 371 Gg (1 Gg = 1000 metric tons) of wet biomass in our time series across central and southern California. By tracking daily changes in biomass, we found that the fraction of kelp canopy biomass that was senescent (> 50 days old) in our study region followed a seasonal cycle; the senescent portion of canopy biomass was lowest in the spring, increased through the summer and peaked in the fall (Figure 4b).

We applied our observed dry-mass normalized DOC_{ex} rates to the satellite-derived estimates of giant kelp canopy biomass and physiological state. We used rates from our dark and light saturating incubations for mature kelp (mean ± 1SD = 0.9 ± 1.0 and 3.3 ± 2.0 μmol C g_{DW}^{-1} hr^{-1}, respectively) and given our observation of no relationship between senescent kelp DOC_{ex} and light intensity, we assumed DOC_{ex} from senescent kelp (mean ± 1SD = 14.0 ± 14.1 μmol C g_{DW}^{-1} hr^{-1}) did not follow a 12-hour light/dark cycle. The uncertainty in these rates was

accounted for by bootstrap analysis with 100,000 simulations. We generated probability distributions and bootstrap statistics (median ± standard error; 95% confidence intervals) for mature, dark DOC_{ex} (0.7 ± 0.3 μmol C g_{DW}^{-1} hr^{-1}; 0.2 – 1.3 μmol C g_{DW}^{-1} hr^{-1}), mature, light saturating DOC_{ex} (3.2 ± 0.3 μmol C g_{DW}^{-1} hr^{-1}; 2.6 – 3.8 μmol C g_{DW}^{-1} hr^{-1}), and senescent DOC_{ex} (6.5 ± 2.2 μmol C g_{DW}^{-1} hr^{-1}; 4.6 – 12.7 μmol C g_{DW}^{-1} hr^{-1}). The medians and 95% confidence intervals were extrapolated to monthly estimates of giant kelp canopy biomass and physiology (Figure 4) across the central and southern California coast, including the California Channel Islands (Figure 5a). Monthly rates were summed to generate annual DOC production rates for giant kelp between 2001-2023 (Figure 5b).

By applying a binary physiological state (mature or senescent) to our estimates of giant kelp canopy biomass, annual DOC production rates increased on average two-fold compared to when we did not account for senescence (Figure 5b). Annual DOC production rates for giant kelp averaged (± 1SD) 4.4 ± 1.9 and 2.1 ± 0.9 Gg C yr^{-1}, with and without including senescence, respectively. On average, the contribution from senescence-driven DOC release would account for 74 ± 3% of total annual DOC production by giant kelp.

Discussion

Coastal vegetated ecosystems are recognized for their outsized contribution to carbon storage[40]. However, the role of marine macroalgae in carbon sequestration remains contentious[14,15]. A potential pathway for macroalgae carbon sequestration may be the amount that is exported as DOC [12,13,41], however this is poorly constrained. Current estimates of global DOC production by macroalgae apply rate measurements from short-term incubations, with macroalgae of unknown physiological condition[42], to some measured or assumed standing stock

of macroalgal biomass [12]. However macroalgal biomass varies seasonally and interannually [43,44], and following periods of growth, biomass physiology can change rapidly due to processes such as senescence or nutrient limitation [30,45]. In our study, we demonstrate that knowledge of kelp's physiological condition, in addition to estimates of standing biomass, greatly improves our understanding of DOC production by kelp and its contributions to coastal carbon budgets.

Seasonal and age-driven changes in physiology and giant kelp senescence

Macroalgae physiology can vary widely across temporal and spatial scales [29,46] .We used tissue C:N and Chl:C ratios as proxies for giant kelp nutrient stress and physiological state, respectively across seasonal and age-driven gradients. Together, the observed age-dependent decline in photosynthetic rates and Chl:C, and increase in C:N, is consistent with the dynamics of progressive senescence in giant kelp populations, and autotrophs in general [25,30,33]. In both seasons, the increase in tissue C:N began after 50 days, suggesting kelp ceases to invest nitrogen resources in blades near the end of their lifespan. Progressive senescence has been studied extensively in terrestrial plants [25,47], however, it has only recently been studied in macroalgae species such as giant kelp [28,33].

The most striking feature of our photosynthetic rate measurements presented was the linear decline in maximum photosynthetic rate with age in both cohorts (Figure 1b), which has been observed previously for giant kelp [33]. Linear age-related declines in maximum photosynthetic rate are consistent with the predictions of leaf-lifespan theory [48]. This theory posits that leaves, and in the case of giant kelp, blades, seek to maximize their photosynthetic gains against the cost of biosynthesis and maintenance. It predicts that leaf lifespans are shorter when initial photosynthetic rates are high and longer when biosynthesis costs are higher or initial

370 photosynthetic rates are low. Our results are consistent with this theory as we observed a more
371 rapid decline in maximum photosynthetic rates in the summer, when the tissue C:N ratio was
372 highest, and a slower decline in the spring when the tissue C:N ratio was lowest (Supplemental
373 Figure 1b). Of important relevance to this study, we observed that this age-related senescence
374 resulted in a large increase in DOC_{ex} by giant kelp (Figure 2b).
375
376 *DOC_{ex}, photosynthetic rate, and light*
377 We observed high variability in hourly DOC_{ex}, for the mature and senescent kelp blade
378 incubations, ranging from -1.2 to 8.1 and 0.2 to 65.3 μmol C g_{DW}^{-1} hr^{-1}, respectively
379 (Supplemental Table 1). For mature kelp, this variability was driven by rates of photosynthesis
380 (Figure 2a), which was a function of both age and light (Figure 1b). Sampled kelp blades were
381 each incubated across limiting (0-300 μmol m^{-2} s^{-1}) and light-saturating intensities (300-1517
382 μmol m^{-2} s^{-1}) for 2-3 hours, and in mature kelp incubations, DOC_{ex} was linearly correlated to
383 NPP, even at light intensities higher than the saturating irradiance (Figure 2a). This indicates that
384 the rate of DOC_{ex} responds rapidly to changes in light but is ultimately constrained by the rate of
385 photosynthesis. This result is consistent with the only other macroalgae study we are aware of
386 that measured simultaneous changes in DOC_{ex} and photosynthesis in response to rapid changes
387 in light[49] . That study found a similar percent extracellular release (PER ~2%) across the same
388 range of light levels. Therefore, models that assume a simple linear relationship with light, may
389 overestimate the proportion of NPP released as DOC by non-senescent macroalgae, as DOC_{ex}
390 would continue to increase beyond light intensities where NPP is light-saturated. One such
391 model was used by Reed et al., (2015)[9], who estimate that giant kelp releases on average 14% of
392 NPP as DOC annually, higher than our average measured PER (~2-3%). In their study, they did

not measure DOC_{ex} and NPP simultaneously, but rather combined mass normalized DOC_{ex} using a simple linear relationship with light with an existing model of giant kelp NPP. Further, they do not differentiate DOC_{ex} by mature or senescent kelp, which, coupled with a simple linear light-DOC_{ex} relationship, may explain their higher estimated PER.

DOC exudation mechanisms of mature kelp

One of the main models for DOC exudation by autotrophs, known as the overflow hypothesis[23] predicts that as algae become nutrient stressed, a greater proportion of recently fixed carbon is released as DOC. According to this hypothesis, algae will release photosynthate in greater proportions relative to NPP when light and nutrients are uncoupled. In our study, we observed a nearly 3-fold difference in the tissue C:N of mature blades between the spring and summer (C:N ~10 - 30), a difference that spans the long-term observations of giant kelp stoichiometry at our study site (Supplemental Table 1, Supplemental Figure 5). Summertime tissue C:N (~30) values were close to the observed maximum for giant kelp at our study site indicating extreme nitrogen depletion [35,50], while springtime tissue C:N values (~10) were typical for this time of year at our study site (Supplemental Figure 5). However, DOC release rates, as a fraction of NPP, by mature blades remained relatively constant across variable tissue C:N (Supplemental Figure 2a), contrary to the predictions of the overflow hypothesis. A possible explanation for a relatively small and constant percent extracellular release (PER) despite a large range in tissue C:N is the body plan of giant kelp. Giant kelp and several other brown macroalgae contain phloem-like transport networks capable of transporting carbohydrates such as glucose and mannitol over a meter per day [51,52]. Unlike phytoplankton, for whom the overflow hypothesis was initially proposed, kelps are multicellular and can transport excess photosynthate

to tissue beneath the canopy that may be light-limited. In the interior of a giant kelp forest, light intensity only a few meters beneath the surface can be less than <10 μmol m^{-2} s^{-1}, several hundred times lower than surface irradiances [33]. Therefore, the release of excess giant kelp photosynthate as DOC by canopy blades in the surface would deprive the biomass below the canopy that relies on this excess photosynthate as a carbon source. In a study of resource translocation of carbon by giant kelp, it was found that canopy blades, like the blades studied here, are important sources of carbon for new frond growth [53]. We hypothesize that DOC release by giant kelp serves an alternative function to energy dissipation and could include the release of DOC for UV protection[54], herbivory deterrence[55], the establishment of their microbiome[56], or drag reduction[57].

Senescence results in the solubilization of kelp biomass

Senescence is known to play a major role in the spatial distribution and biomass of primary producers [28,47], yet, its role in partitioning biomass between dissolved and particulate detritus has not been previously studied. DOC_{ex} rates for senescent kelp blades were considerably higher than observed for mature kelp and were uncoupled from rates of photosynthesis and light intensity (Figure 2b). DOC_{ex} during senescence increased with the level of physiological decline of the kelp tissue which generally increased with age after the onset of senescence (Supplemental Figure 4). Comparatively, DOC_{ex} rates often exceeded the simultaneous rate of NPP during senescence (Figure 2b), indicating the loss of previously fixed carbon as DOC through solubilization (i.e. the transformation of particulate organic carbon into DOC), rather than by direct exudation. This apparent solubilization of kelp biomass was supported in our analysis of the dissolved carbohydrates released by giant kelp (Figure 3a) and

439 the positive relationship between DOC_{ex} and the proportion of mannuronic acid (Man-URA) in
440 released dissolved carbohydrates (Figure 3b). Man-URA is one of the two acidic sugars (with
441 guluronic acid) in alginate, a carbohydrate that makes up to half of kelp biomass and is a major
442 cell wall polymer [58]. The enrichment of Man-URA in the dissolved exudates, coupled with high
443 DOC_{ex} relative to NPP after 50 days indicates the solubilization of alginate into the dissolved
444 phase.

445 Despite the observed solubilization of biomass in kelp older than 50 days, senescent kelp
446 blades were not dead and continued to photosynthesize, albeit at lower rates (Figure 1b,
447 Supplemental Figure 1b). A possible cause for the progressive solubilization of kelp tissue
448 following the onset of senescence is the growth of epiphytic bacteria, whose hydrolytic enzymes
449 breakdown structural compounds. Kelps contain little cellulose and no lignin, but maintains the
450 structural integrity of their cell walls with a combination of sulfated carbohydrates, such as
451 fucoidan, and carbohydrates rich in acidic sugars, such as alginate [59]. Bacteria are abundant on
452 the surfaces of kelp, and in studies of decaying brown algae, epiphytic bacteria prioritize the
453 degradation of alginate over other structural carbohydrates [60,61]. This degradation is performed
454 by bacteria that are initially rare on the surfaces of the kelp [62], suggesting that as kelp age,
455 microbiome disruption can enhance tissue degradation. Indeed, as part of a complimentary
456 study[63] we observed changes in giant kelp's microbiome during senescence; including an
457 increase in the relative abundance of members of the Flavobacteria and Proteobacteria, two
458 groups enriched in alginate degrading bacteria[64]. Although some bacterial alginate lyase enzymes
459 are tethered to the cell surface (ectoenzymes) to allow efficient scavenging of the hydrolyzed
460 sugars, some bacteria use untethered enzymes (exoenzymes) that can result in the efflux of
461 degradation products like smaller poly- and oligosaccharides [65,66]. The broadcasting of alginate

lyase enzymes by epiphytic bacteria may be responsible for the observed solubilization of kelp biomass in our study, ultimately resulting in a pulse of DOC into the surrounding seawater during kelp senescence. This process is well-described in sinking marine particulate organic matter, were bacteria solubilize polymers faster than products can be taken up, resulting in plumes of DOC [67–69]. We propose that solubilization is a major avenue for giant kelp biomass transformation into the marine DOC pool.

Incorporation of senescence into estimates of kelp forest DOC production

Giant kelp grows year-round; however, growth rates and biomass are linked to changing environmental conditions, such as light and nutrient availability and intrinsic factors, including senescence [28,43]. As a result, a single giant kelp forest stand can have a wide range of blade ages[30]. We observed that at large scales, giant kelp biomass generally follows a seasonal pattern of rapid growth between the spring and summer, followed by a decline through the fall and winter (Figure 4a), due to senescence and wave disturbances [28,43]. The fraction of senescent blades peaks in the fall, three months after the peak in giant kelp biomass, where on average 68 ± 10% of the total canopy biomass is senescent (Figures 4a and 4b). By incorporating a simple binary age structure into our regional observations of giant kelp canopy biomass (Figure 5a), we found that senescence-driven solubilization is responsible for, on average, 74% of annual giant kelp DOC production. At the upper range, giant kelp potentially contributes up to 8.2 Gg C yr^{-1} (range = 5.8 – 14.8 Gg C yr^{-1}) as DOC to the coastal ocean in central and southern California (Figure 5b); a small amount of carbon compared to other sources of DOC to the coastal ocean, such as rivers, the largest of which deliver between 230 – 26,900 Gg C yr^{-1} $river^{-1}$ (global total ~ 250 Tg C yr^{-1}) [70].

Our study covers only one kelp forest species in a single region where giant kelp canopies has been observed from satellite imagery (up to ~50 km^2 of giant kelp canopy). This is a small fraction of the total potential kelp forest area globally (potential area ~ 1.96 million km^2)[10]. A simple extrapolation of our maximum regional giant kelp DOC production estimate (8.2 (range = 5.8 – 14.8) Gg C yr^{-1} / 50 km^2) to this potential area would equal a global kelp forest DOC production rate of 321 (227-580) Tg C yr^{-1}. This is roughly six times higher than estimates of kelp forest particulate organic carbon export (~56 Tg C yr^{-1})[10], and is equivalent to global DOC production for all macroalgae, not just kelp forests, estimated by Krause-Jensen & Duarte (2016) (330 Tg C yr^{-1}). However, it is important to note that this estimate assumes kelp forests occupy all available, habitable space[8,10] and therefore represents an upper limit for global kelp DOC production. This assumption is likely rarely, if ever met. For example, our observations of giant kelp canopy biomass show large intra- and interannual variability for a single region; standing canopy biomass at any given time between 2001 – 2023 is on average (± 1 SD) only 23 ± 19% of the maximum observed biomass in August 2005 (Figure 4a). Further, kelp forests are declining around the globe as a result of anthropogenic forces and marine heatwaves [71,72], making it less likely that kelp forests will reach their maximum potential biomass. Future work should prioritize constraining uncertainties in modelled macroalgae biomass and area using *in situ* observations and remote sensing as part of multi-annual, year-round studies.

Conclusions & implications for integrating macroalgae into blue carbon estimates

This study demonstrates that consideration of physiology is needed to constrain the pathways and fate of macroalgal-derived carbon in the coastal ocean. While not all macroalgae

undergo progressive senescence in the same way as giant kelp, there is evidence for seasonal senescence in year-round surveys of other macroalgae species [44,45,73,74]. For example, pelagic *Sargassum* forms extensive blooms in the western North Atlantic and Caribbean Sea, totaling up to 20,000 Gg of wet biomass[44]. After the bloom peaks in the summer, there is a rapid decline in *Sargassum* biomass between July and December, a similar pattern we observed for giant kelp (Figure 4a). Additionally, three previous studies[19,21,45], encompassing seven species of brown macroalgae (*Ascophyllum nodosum, Fucus vesiculosus, Fucus serratus, Laminaria saccharina, Rhodimenia palmata, Saccharina japonica, Ecklonia cava)* observed elevated DOC release rates in the summer and fall compared to the rest of the year, suggesting that enhanced DOC production as a result of seasonal senescence may be a common feature of macroalgae. This is important to consider for blue carbon estimates, as it would increase the amount of biomass estimated to be exported as DOC, rather than particulate organic carbon, limiting the downward flux of macroalgal organic carbon necessary for sequestration. Future work should determine whether our observed DOC_{ex} rates and seasonal patterns related to senescence can be generalized to all macroalgae.

Acknowledgments

We thank the invaluable work of members of the Santa Barbara Coastal LTER whose data provided important background for our findings. We thank all Carlson lab members for the valuable discussion on the data. We thank A. Santoro for her constructive comments and discussion of the data and manuscript. This project was funded by the Department of Energy's Advanced Research Project Agency-Energy through award DE-AR0001559 to TWB, DAS and CAC, and the National Science Foundation's Santa Barbara Coastal LTER through award number OCE-1831937 to DAS and CAC.

Data & Code Availability

Data and code used for data analysis, statistics and figure generations is available at https://github.com/chance-english/Giant_Kelp_DOC. Code for Landsat multispectral imagery of giant kelp canopy biomass and age is available upon request.

References

1. Carlson, C. A., Liu, S., Stephens, B. M. & English, C. J. DOM production, removal, and transformation processes in marine systems. in *Biogeochemistry of Marine Dissolved Organic Matter* 137–246 (Elsevier, 2024). doi:10.1016/B978-0-443-13858-4.00013-7.
2. Duarte, C. M., Middelburg, J. J. & Caraco, N. Major role of marine vegetation on the oceanic carbon cycle. *Biogeosciences* **2**, 1–8 (2005).
3. Watanabe, K. *et al.* Macroalgal metabolism and lateral carbon flows can create significant carbon sinks. *Biogeosciences* **17**, 2425–2440 (2020).
4. Macreadie, P. I. *et al.* The future of Blue Carbon science. *Nat. Commun.* **10**, 3998 (2019).
5. Committee on A Research Strategy for Ocean-based Carbon Dioxide Removal and Sequestration, Division on Earth and Life Studies, & National Academies of Sciences, Engineering, and Medicine. *A Research Strategy for Ocean-Based Carbon Dioxide Removal and Sequestration*. 26278 (National Academies Press, Washington, D.C., 2021). doi:10.17226/26278.
6. Eger, A. *et al.* The Kelp Forest Challenge: A collaborative global movement to protect and restore 4 million hectares of kelp forests. *J. Appl. Phycol.* **36**, 951–964 (2024).
7. Macreadie, P. I. *et al.* Blue carbon as a natural climate solution. *Nat. Rev. Earth Environ.* **2**, 826–839 (2021).
8. Duarte, C. M. *et al.* Global estimates of the extent and production of macroalgal forests. *Glob. Ecol. Biogeogr.* **31**, 1422–1439 (2022).
9. Smith, S. V. Marine Macrophytes as a Global Carbon Sink. *Sci. New Ser.* **211**, 838–840 (1981).

10. Filbee-Dexter, K. *et al.* Carbon export from seaweed forests to deep ocean sinks. *Nat. Geosci.* **17**, 552–559 (2024).
11. Reed, D. C. *et al.* Patterns and controls of reef-scale production of dissolved organic carbon by giant kelp Macrocystis pyrifera. *Limnol. Oceanogr.* **60**, 1996–2008 (2015).
12. Krause-Jensen, D. & Duarte, C. M. Substantial role of macroalgae in marine carbon sequestration. *Nat. Geosci.* **9**, 737–742 (2016).
13. Watanabe, K. *et al.* Macroalgal metabolism and lateral carbon flows can create significant carbon sinks. 16 (2020).
14. Bach, L. T. *et al.* Testing the climate intervention potential of ocean afforestation using the Great Atlantic Sargassum Belt. *Nat. Commun.* **12**, 2556 (2021).
15. Hurd, C. L. *et al.* Forensic carbon accounting: Assessing the role of seaweeds for carbon sequestration. *J. Phycol.* **58**, (2022).
16. Brylinsky, M. Release of dissolved organic matter by some marine macrophytes. *Mar. Biol.* **39**, 213–220 (1977).
17. Carlson, D. J. & Carlson, M. L. Reassessment of exudation by fucoid macroalgae. *Limnol. Oceanogr.* **29**, 1077–1087 (1984).
18. Hanson, R. B. Pelagic Sargassum community metabolism: Carbon and nitrogen. *J. Exp. Mar. Biol. Ecol.* **29**, 107–118 (1977).
19. Khailov, K. M. & Burlakova, Z. P. Release of Dissolved Organic Matter by Marine Seaweeds and Distribution of Their Total Organic Production to Inshore Communities. *Limnol. Oceanogr.* **14**, 521–527 (1969).

20. Mueller, B., den Haan, J., Visser, P. M., Vermeij, M. J. A. & van Duyl, F. C. Effect of light and nutrient availability on the release of dissolved organic carbon (DOC) by Caribbean turf algae. *Sci. Rep.* **6**, 23248 (2016).
21. Wada, S. *et al.* Quantitative and qualitative analyses of dissolved organic matter released from Ecklonia cava Kjellman, in Oura Bay, Shimoda, Izu Peninsula, Japan. *J. Exp. Mar. Biol. Ecol.* **349**, 344–358 (2007).
22. Weigel, B. L. & Pfister, C. A. The dynamics and stoichiometry of dissolved organic carbon release by kelp. *Ecology* **102**, (2021).
24. Paine, E. R. *et al.* Strong seasonal patterns of DOC release by a temperate seaweed community: Implications for the coastal ocean carbon cycle. *J. Phycol.* **59**, 738–750 (2023).
25. Thomas, H. Senescence, ageing and death of the whole plant. *New Phytol.* **197**, 696–711 (2013).
26. Bidle, K. D. Programmed Cell Death in Unicellular Phytoplankton. *Curr. Biol.* **26**, R594–R607 (2016).
27. Bell, T. W., Allen, J. G., Cavanaugh, K. C. & Siegel, D. A. Three decades of variability in California's giant kelp forests from the Landsat satellites. *Remote Sens. Environ.* **238**, 110811 (2020).
28. Rodriguez, G. E., Rassweiler, A., Reed, D. C. & Holbrook, S. J. The importance of progressive senescence in the biomass dynamics of giant kelp (Macrocystis pyrifera). *Ecology* **94**, 1848–1858 (2013).
29. Bell, T. W., Reed, D. C., Nelson, N. B. & Siegel, D. A. Regional patterns of physiological condition determine giant kelp net primary production dynamics. *Limnol. Oceanogr.* **63**, 472–483 (2018).

30. Bell, T. W. & Siegel, D. A. Nutrient availability and senescence spatially structure the dynamics of a foundation species. *Proc. Natl. Acad. Sci.* **119**, e2105135118 (2022).
31. Yorke, C., Miller, R., Page, H. & Reed, D. Importance of kelp detritus as a component of suspended particulate organic matter in giant kelp Macrocystis pyrifera forests. *Mar. Ecol. Prog. Ser.* **493**, 113–125 (2013).
32. Seely, G. R., Duncan, M. J. & Vidaver, W. E. Preparative and analytical extraction of pigments from brown algae with dimethyl sulfoxide. *Mar. Biol.* **12**, 184–188 (1972).
33. Rodriguez, G. E., Reed, D. C. & Holbrook, S. J. Blade life span, structural investment, and nutrient allocation in giant kelp. *Oecologia* **182**, 397–404 (2016).
34. Zimmerman, R. C. & Kremer, J. N. In situ growth and chemical composition of the giant kelp, Macrocystis pyrifera: response to temporal changes in ambient nutrient availability. *Mar. Ecol. Prog. Ser.* **27**, 277–285 (1986).
35. Gerard, V. A. Growth and utilization of internal nitrogen reserves by the giant kelp Macrocystis pyrifera in a low-nitrogen environment. *Mar. Biol.* **66**, 27–35 (1982).
36. Wheeler, W. N. Pigment content and photosynthetic rate of the fronds of Macrocystis pyrifera. *Mar. Biol.* **56**, 97–102 (1980).
37. Bockmon, E. E. & Dickson, A. G. An inter-laboratory comparison assessing the quality of seawater carbon dioxide measurements. *Mar. Chem.* **171**, 36–43 (2015).
38. Halewood, E. *et al.* Determination of dissolved organic carbon (DOC) and total dissolved nitrogen (TDN) in seawater using High Temperature Combustion Analysis. *Ocean Best Pract. Repos.* 52 (2022) doi:http://dx.doi.org/10.25607/OBP-1745.

641 39. Engel, A. & Händel, N. A novel protocol for determining the concentration and composition
642 of sugars in particulate and in high molecular weight dissolved organic matter (HMW-DOM)
643 in seawater. *Mar. Chem.* **127**, 180–191 (2011).
644 40. Rosentreter, J. A. *et al.* Coastal vegetation and estuaries are collectively a greenhouse gas
645 sink. *Nat. Clim. Change* **13**, 579–587 (2023).
646 41. Buck-Wiese, H. *et al.* Fucoid brown algae inject fucoidan carbon into the ocean. *Proc. Natl.*
647 *Acad. Sci.* **120**, e2210561119 (2023).
648 42. Barrón, C., Apostolaki, E. T. & Duarte, C. M. Dissolved organic carbon fluxes by seagrass
649 meadows and macroalgal beds. *Front. Mar. Sci.* **1**, (2014).
650 43. Reed, D. C., Rassweiler, A. & Arkema, K. K. Biomass Rather Than Growth Rate Determines
651 Variation in Net Primary Production by Giant Kelp. *Ecology* **89**, 2493–2505 (2008).
652 44. Wang, M. *et al.* The great Atlantic Sargassum belt. *Science* **365**, 83–87 (2019).
653 45. Carlson, A. K., Yoshimura, T. & Kudo, I. Kelp dissolved organic carbon release is seasonal
654 and annually enhanced during senescence. *J. Phycol.* **60**, 980–1000 (2024).
655 46. Lapointe, B. E. A comparison of nutrient-limited productivity in Sargassum natans from
656 neritic vs. oceanic waters of the western North Atlantic Ocean. *Limnol. Oceanogr.* **40**, 625–
657 633 (1995).
658 47. Leopold, A. C. Senescence in Plant Development. *Science* **134**, 1727–1732 (1961).
659 48. Kikuzawa, K. A Cost-Benefit Analysis of Leaf Habit and Leaf Longevity of Trees and Their
660 Geographical Pattern. *Am. Nat.* **138**, 1250–1263 (1991).
661 49. Zhao, Z.-F. *et al.* Effects of instantaneous changes in temperature, light, and salinity on the
662 dynamics of dissolved organic carbon release by Sargassum thunbergii. *Mar. Pollut. Bull.*
663 **190**, 114865 (2023).

50. Brzezinksi, M. *et al.* Multiple Sources and Forms of Nitrogen Sustain Year-Round Kelp Growth on the Inner Continental Shelf of the Santa Barbara Channel. *Oceanography* **26**, 114–123 (2013).
51. Drobnitch, S. T., Jensen, K. H., Prentice, P. & Pittermann, J. Convergent evolution of vascular optimization in kelp (Laminariales). *Proc. R. Soc. B Biol. Sci.* **282**, 20151667 (2015).
52. Schmitz, K. & Lobban, C. S. A survey of translocation in laminariales (Phaeophyceae). *Mar. Biol.* **36**, 207–216 (1976).
53. Fox, M. D. Resource translocation drives ^{13} C fractionation during recovery from disturbance in giant kelp, *Macrocystis pyrifera*. *J. Phycol.* **49**, 811–815 (2013).
54. Powers, L. C. *et al.* Sargassum sp. Act as a Large Regional Source of Marine Dissolved Organic Carbon and Polyphenols. *Glob. Biogeochem. Cycles* **33**, 1423–1439 (2019).
55. Jennings, J. G. & Steinberg, P. D. In situ exudation of phlorotannins by the sublittoral kelp Ecklonia radiata. *Mar. Biol.* **121**, 349–354 (1994).
56. Egan, S. *et al.* The seaweed holobiont: understanding seaweed–bacteria interactions. *FEMS Microbiol. Rev.* **37**, 462–476 (2013).
57. Hoyt, J. W. High molecular weight algal substances in the sea. *Mar. Biol.* **7**, 93–99 (1970).
58. Kloareg, B. & Quatrano, R. Structure of the cell walls of marine algae and ecophysiological functions of the matrix polysaccharides. *Oceanogr. Mar. Biol. Annu. Rev.* **26**, 259–315 (1988).
59. Shao, Z. & Duan, D. The Cell Wall Polysaccharides Biosynthesis in Seaweeds: A Molecular Perspective. *Front. Plant Sci.* **13**, 902823 (2022).

686 60. Zhang, Y.-S. *et al.* Metagenomic insights into the dynamic degradation of brown algal
687 polysaccharides by kelp-associated microbiota. *Appl. Environ. Microbiol.* **90**, e02025-23
688 (2024).
689 61. Zhu, Y. *et al.* Complete genome sequence and transcriptomic analysis of a novel marine
690 strain *Bacillus weihaiensis* reveals the mechanism of brown algae degradation. *Sci. Rep.* **6**,
691 38248 (2016).
692 62. Minich, J. J. *et al.* Elevated temperature drives kelp microbiome dysbiosis, while elevated
693 carbon dioxide induces water microbiome disruption. *PLOS ONE* **13**, e0192772 (2018).
694 63. English, C. J. Biogeochemistry and ecology of macroalgal-derived dissolved organic carbon.
695 Ph.D. Dissertation, University of California, Santa Barbara, Santa Barbara (2024).
696 https://escholarship.org/uc/item/5x1658z4
697 64. Thomas, F. *et al.* Characterization of the first alginolytic operons in a marine bacterium:
698 from their emergence in marine Flavobacteriia to their independent transfers to marine
699 Proteobacteria and human gut Bacteroides. *Environ. Microbiol.* **14**, 2379–2394 (2012).
700 65. Reintjes, G., Arnosti, C., Fuchs, B. & Amann, R. Selfish, sharing and scavenging bacteria in
701 the Atlantic Ocean: a biogeographical study of bacterial substrate utilisation. *ISME J.* **13**,
702 1119–1132 (2019).
703 66. Reintjes, G., Arnosti, C., Fuchs, B. M. & Amann, R. An alternative polysaccharide uptake
704 mechanism of marine bacteria. *ISME J.* **11**, 1640–1650 (2017).
705 67. Alcolombri, U. *et al.* Sinking enhances the degradation of organic particles by marine
706 bacteria. *Nat. Geosci.* **14**, 775–780 (2021).

68. Alldredge, A. L. Interstitial dissolved organic carbon (DOC) concentrations within sinking marine aggregates and their potential contribution to carbon flux. *Limnol. Oceanogr.* **45**, 1245–1253 (2000).

69. Smith, D. C., Simon, M., Alldredge, A. L. & Azam, F. Intense hydrolytic enzyme activity on marine aggregates and implications for rapid particle dissolution. *Nature* **359**, 139–142 (1992).

70. Raymond, P. A. & Spencer, R. G. M. Riverine DOM. in *Biogeochemistry of Marine Dissolved Organic Matter* 509–533 (Elsevier, 2015). doi:10.1016/B978-0-12-405940-5.00011-X.

71. Krumhansl, K. A. *et al.* Global patterns of kelp forest change over the past half-century. *Proc. Natl. Acad. Sci.* **113**, 13785–13790 (2016).

72. Arafeh-Dalmau, N. *et al.* Marine heat waves threaten kelp forests. *Science* **367**, 635–635 (2020).

73. Lüning, K. When do algae grow? The third Founders' lecture. *Eur. J. Phycol.* **29**, 61–67 (1994).

74. Yokohama, Y., Tanaka, J. & Chihara, M. Productivity of theEcklonia cava community in a bay of Izu Peninsula on the Pacific Coast of Japan. *Bot. Mag. Tokyo* **100**, 129–141 (1987).

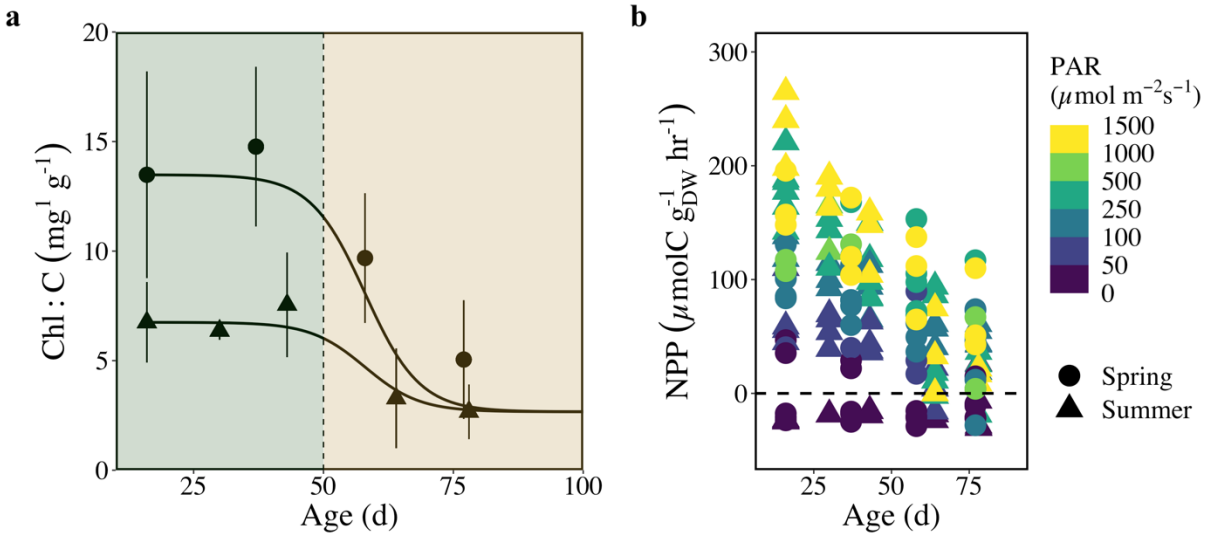

727

728 **Figure 1**. Physiological state and NPP are a function of environmental conditions and age **(a)**
729 Age-related changes in the tissue chlorophyll *a* to carbon ratio in the spring (circles) and summer
730 (triangles). Shading on either side of 50 days represents the transition between mature (<50 days)
731 and senescent (>50 days) giant kelp. Solid lines are a sigmoidal fit to emphasize the non-linear
732 decline in Chl:C with age. Curves were manually fit assuming a maximum age of 100 days and a
733 minimum Chl:C equal to the average Chl:C for the summer cohort at 78 days of age. Error bars
734 are ±1SD from the mean for the six replicate blades sampled for each age. **(b)** Rate of net
735 primary production (NPP) by giant kelp blades in response to gradients in age and light. Trends
736 for the spring (circles) and summer (triangles) are shown. Dashed, horizontal line represents the
737 transition between respiration and photosynthesis.

738

739

740

741

742

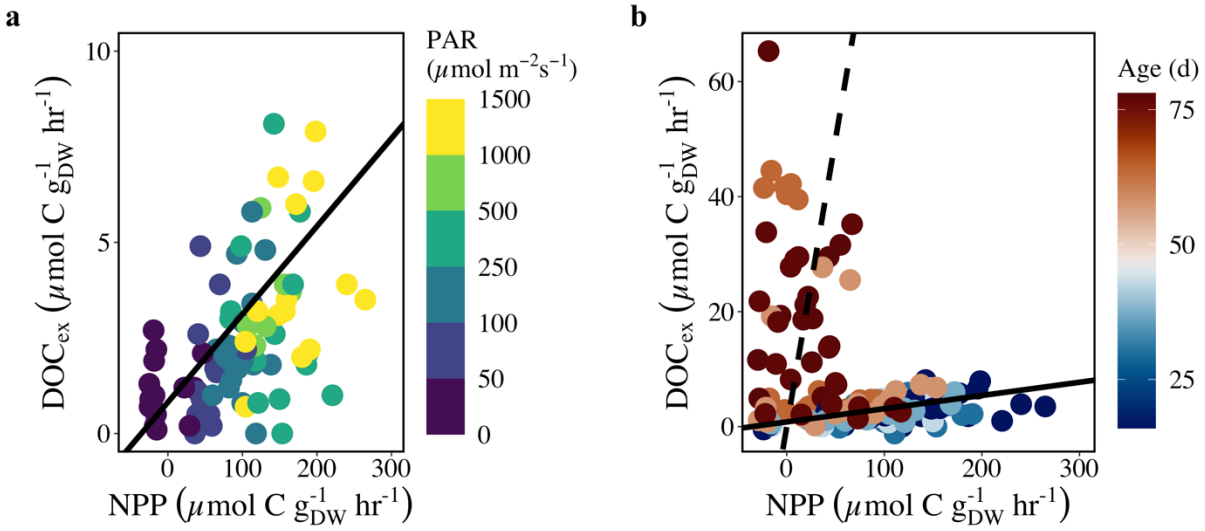

743

744 **Figure 2**. Relationship between DOC exudation (DOC_{ex}) and NPP across environmental and

745 physiological gradeints **(a)** Rates of by mature giant kelp blades (< 50 days of age) vs. NPP over

746 a gradient of light levels. Solid line is the significant linear relationship between DOC_{ex} and NPP

747 for mature blades (Model II, $R^2 = 0.27$, $y = 0.015x + 0.96$, $p < 0.001$). **(b)** The DOC_{ex} vs. NPP

748 relationship across a gradient of blade ages including mature (<50 days) and senescent (> 50

749 days) kelp blades. The solid black line is the regression line from panel A and the dashed line is

750 the 1:1 line. Data points to the left of the dashed line are indicative of kelp tissue solubilization to

751 DOC.

752

753

754

755

756

757

758

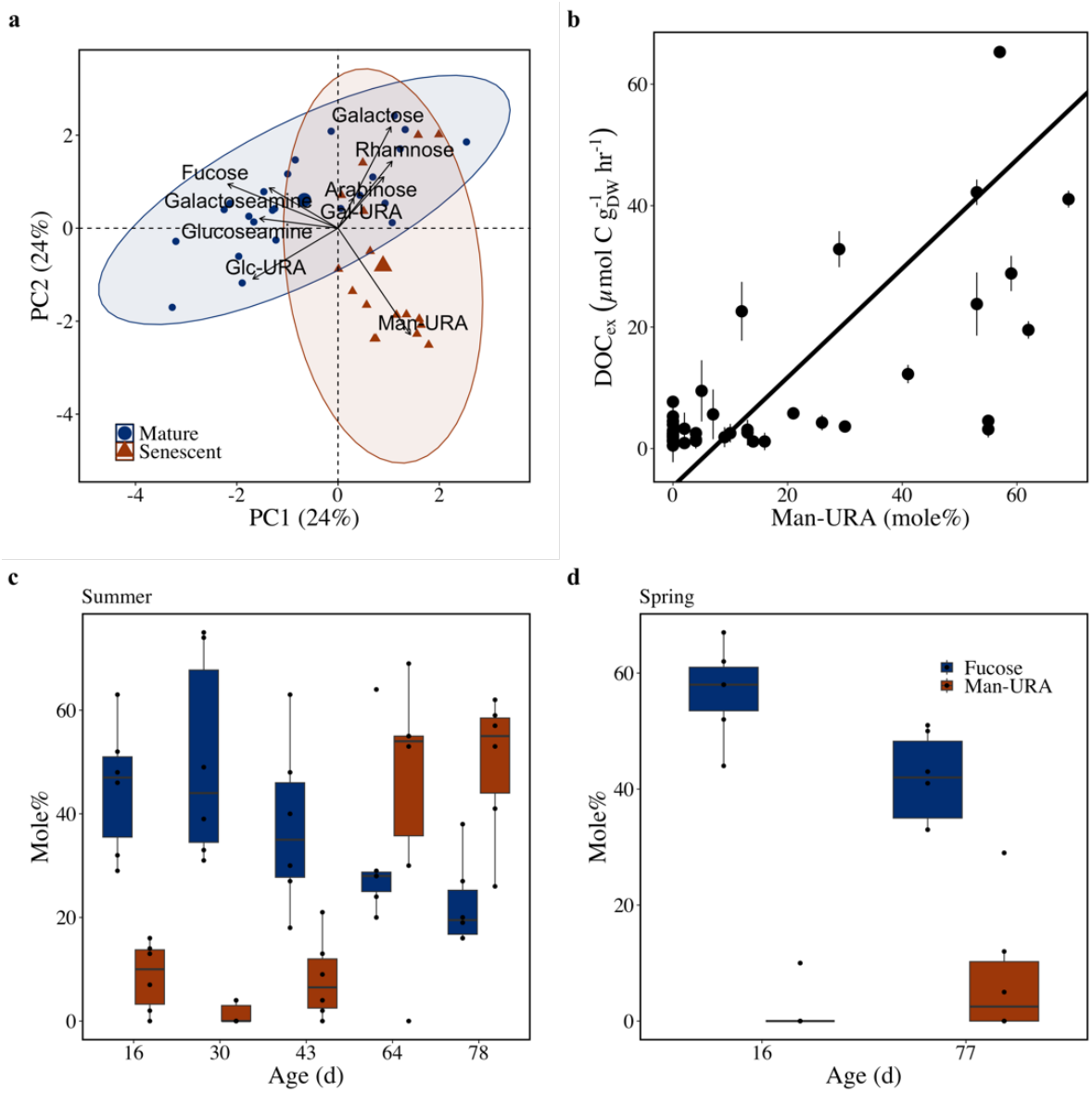

Figure 3. Changes in giant kelp exudate sugar content between physiological states suggest structural carbohydrates such as alginate are being solubilized following senescence. **(a)** Principle component (PC) analysis of giant kelp carbohydrate exudate sugar content expressed as molar percentages between mature and senescent phase kelp. Ellipses represent 95% confidence regions between mature (blue circles) and senescent (red triangles) kelp exudates. Arrow lengths represent the strength of the correlation between each individual sugar monomer to the two principal components (PC1 & PC2) shown. Large points in center of each ellipses are the

centroids. Sugar monomer names are overlayed next to arrows. Abbreviations: Glc-URA (glucuronic acid), Gal-URA (galacturonic acid), Man-URA (mannuronic acid). **(b)** Relationship between rate of DOC production by giant kelp and the mole% of Man-URA in dissolved carbohydrates. Solid line represents the significant Model II regression between the two variables ($y = 89.7*x -6.22$, $R^2 = 0.50$, $p < 0.001$, $n = 42$). Error bars in the y-axis are the ±1 standard deviations from the mean for the DOC production rates by a single blade incubated across multiple light levels (n = 3). **(c)** Mole% of fucose and mannuronic acid (Man-URA) in the summer and **(d)** spring carbohydrates exuded by giant kelp at different ages. Box and whiskers show the interquartile range, with the median and the variability outside the first and second quartiles, respectively. The x-axis is not continuous, and for each discrete age shown on the x-axis there is a value for both the mole% of Fucose and Man-URA.

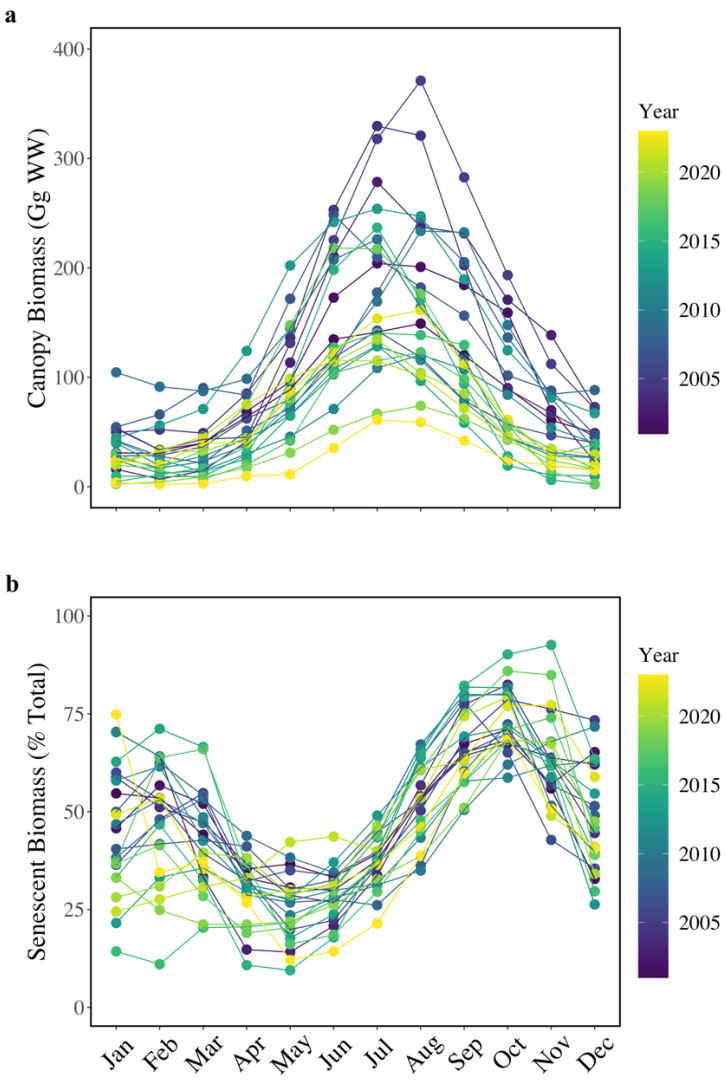

Figure 4: Intra- and interannual variability in giant kelp canopy biomass (in Gg of wet weight) and physiological state estimated from Landsat imagery across the central and southern California region. **(a)** Monthly estimates of giant kelp canopy biomass between 2001-2023 derived from Landsat 7, 8, and 9 multispectral sensors. Note: 1 Gg = 1000 metric tons. **(b)** Percentage of total monthly biomass in panel A that is senescent (> 50 days old). Multiple points in each month are estimates from individual years. In both panels interannual variability is shown by the point and line color.

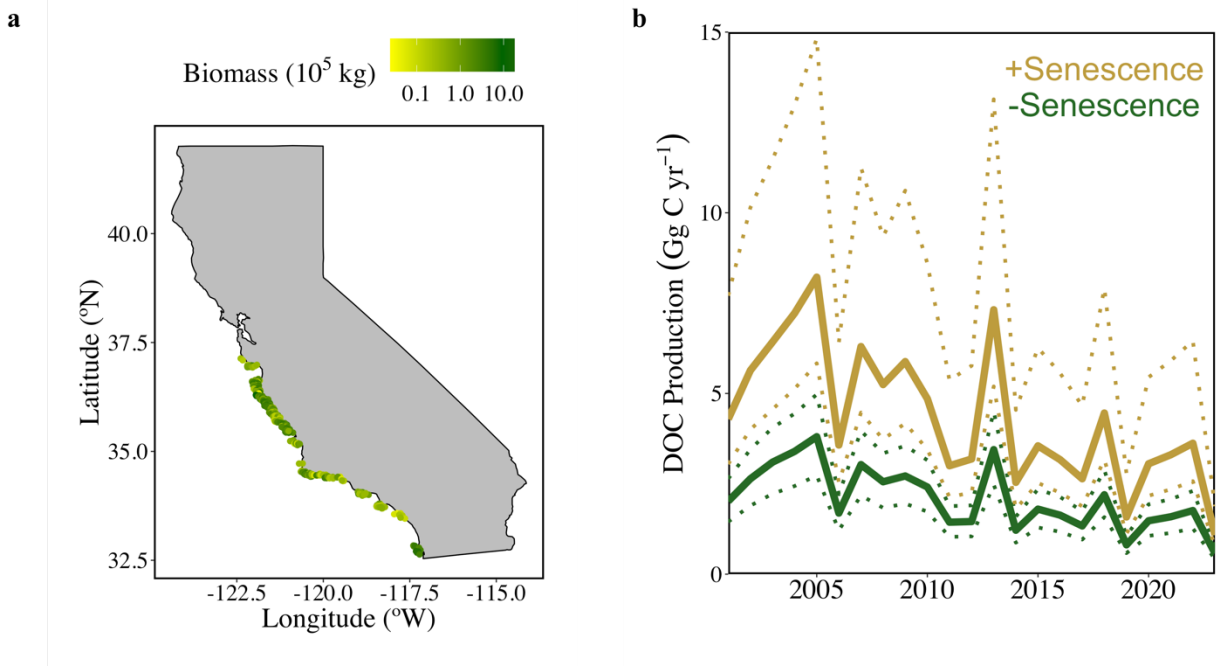

788

789 **Figure 5.** Annual DOC production by giant kelp across central and southern California. **(a)**
790 Average standing giant kelp canopy biomass (in kg of wet weight) in 500m latitudinal bands
791 between years 2000-2023. **(b)** Annual DOC production for the region in panel A between 2000-
792 2023 with (gold lines) and without (green lines) consideration of senescence. Rates were
793 calculated using satellite-derived canopy biomass and age with our mass-specific DOC_{ex} rates
794 derived from our incubations. Solid and dashed lines shows the rates derived from the median
795 and 95% confidence intervals, respectively from the uncertainty analysis of our DOC_{ex} rates.

796

797

798

799

800

801

802

Supplemental Figures

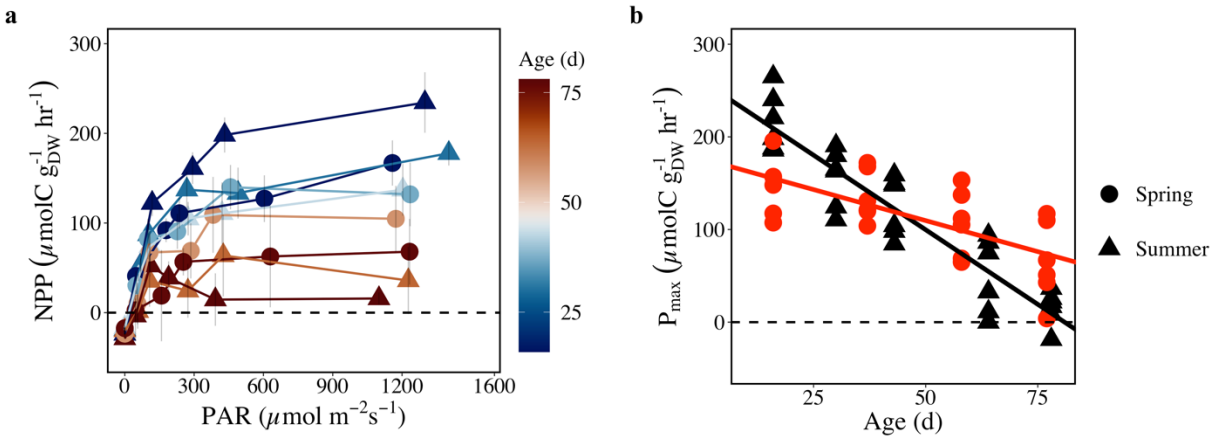

Supplemental Figure 1. (a) Photosynthesis-irradiance curves for giant kelp blades grouped by age and season. Error bars represent ±1SD of DIC uptake rates for triplicate blades incubated at similar light levels. **(b)** Linear decrease in maximum photosynthetic rate (P_{max}) with age in both spring (OLS, $R^2 = 0.44$, $p < 0.001$, $y = -1.33x + 176.6$, $n = 24$) and summer (OLS, $R^2 = 0.85$, $p < 0.001$, $y = -3.22 + 260.7$). Each point is the photosynthetic rate of one of the six blades incubated at a saturating irradiance (> 300 µmol m^{-2} s^{-1}).

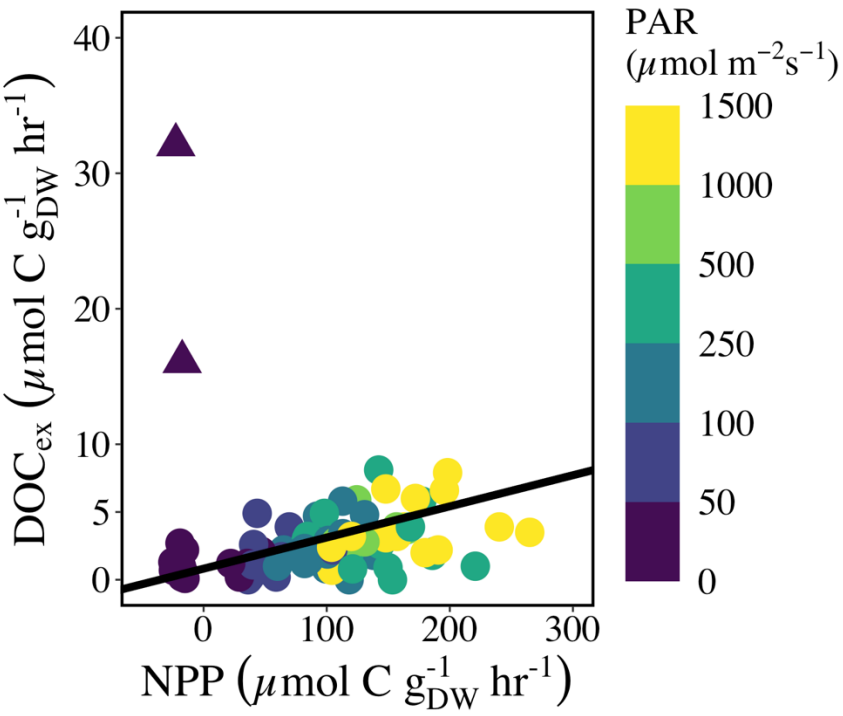

821

822 **Supplemental Figure 2**. Figure 2 in the main text including the two excluded outlier points,
823 shown as triangles. In mature kelp incubations (age < 50 days), two blades were accidently
824 damaged by the stir bar in the incubation chambers, resulting in elevated DOC_{ex} (16.1 & 32.1
825 µmol C g_{DW}^{-1} hr^{-1}) in the dark (PAR = 0). Previous to the damage, in their respective light
826 incubations (PAR = 74 – 554 µmol m^{-2} s^{-1}), these blades had DOC_{ex} rates between -1.2 – 5.9
827 µmol C g_{DW}^{-1} hr^{-1} that fell along the Model II regression line shown.

828

829

830

831

832

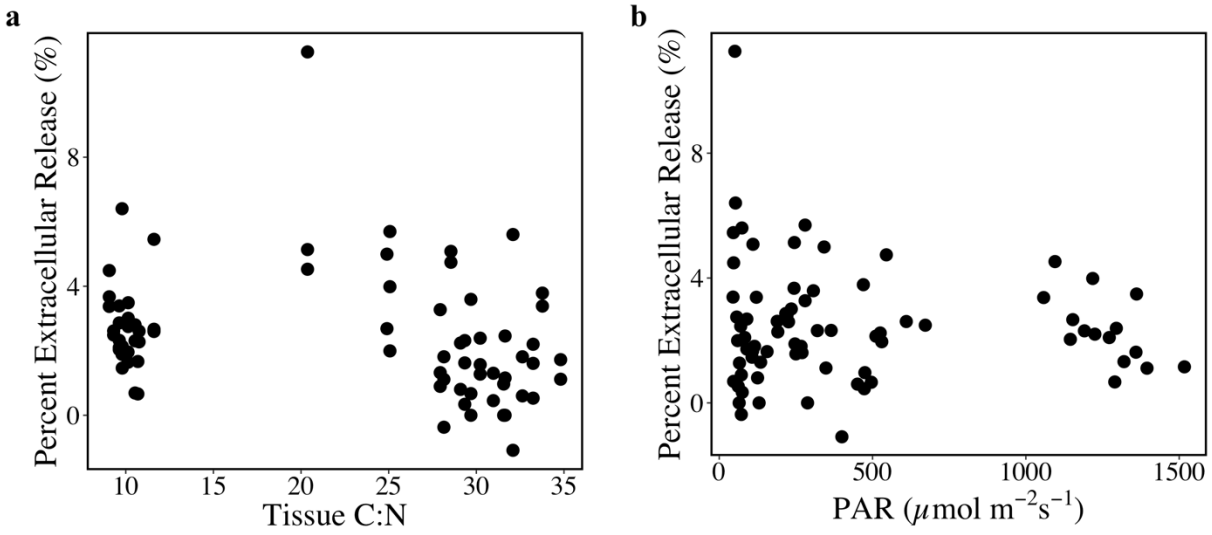

833

834 **Supplemental Figure 3. (a)** There is a weak negative, significant relationship (Model II, $p <$

835 0.001, $R^2 = 0.08$) between the percent extracellular release (DOC/NPP *100%) of mature kelp

836 blades (age < 50 days) and Tissue carbon to nitrogen content (C:N), **(b)** There is no significant

837 correlation between PER of mature kelp blades and light intensity

838

839

840

841

842

843

844

845

846

847

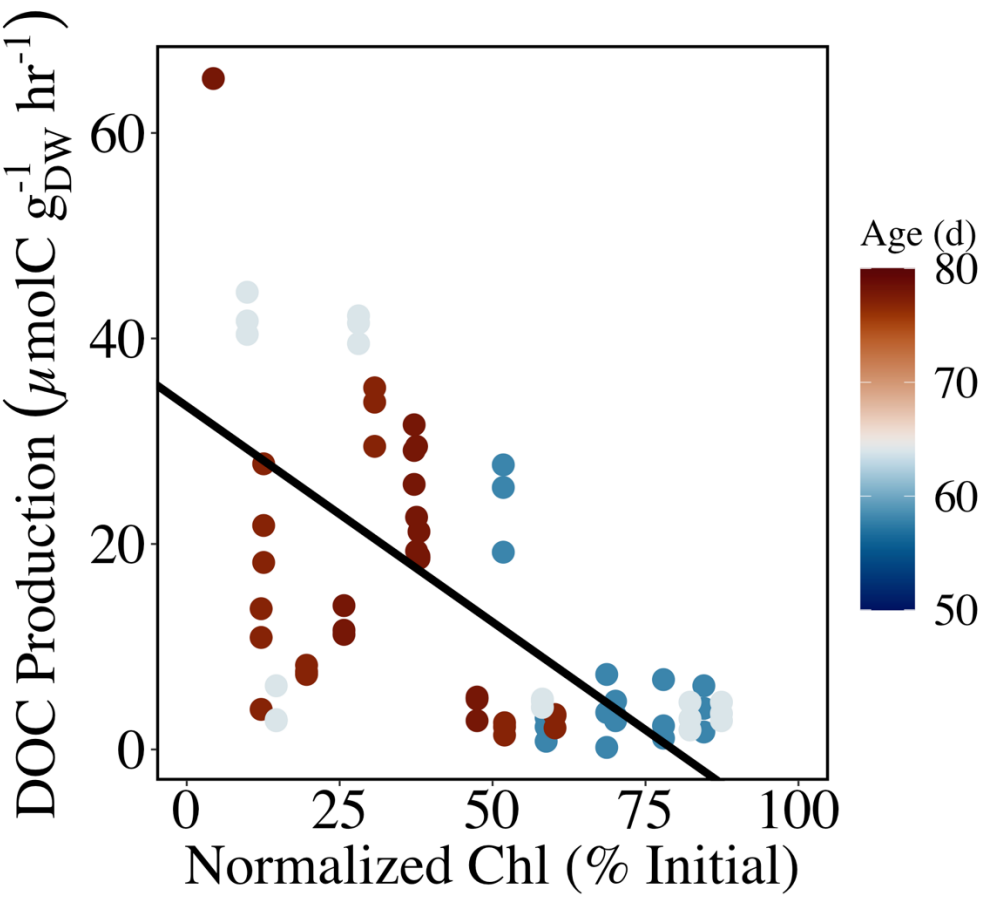

848

849 **Supplemental Figure 4.** DOC production by senescent phase kelp (>50 days of age) increases

850 with the progressive physiological decline in kelp blade chlorophyll *a* (Chl*a*) content.

851 Normalized Chl*a* content is the Chl*a* content of each blade (age > 50 days) expressed as a

852 percent of the average Chl*a* content at the beginning of each cohort sampling (age = 16 days).

853 Solid line is the significant model II regression result ($y = -0.42x + 33.4$, $R^2 = 0.35$, $p = 4.1e^{-08}$).

854

855

856

857

858

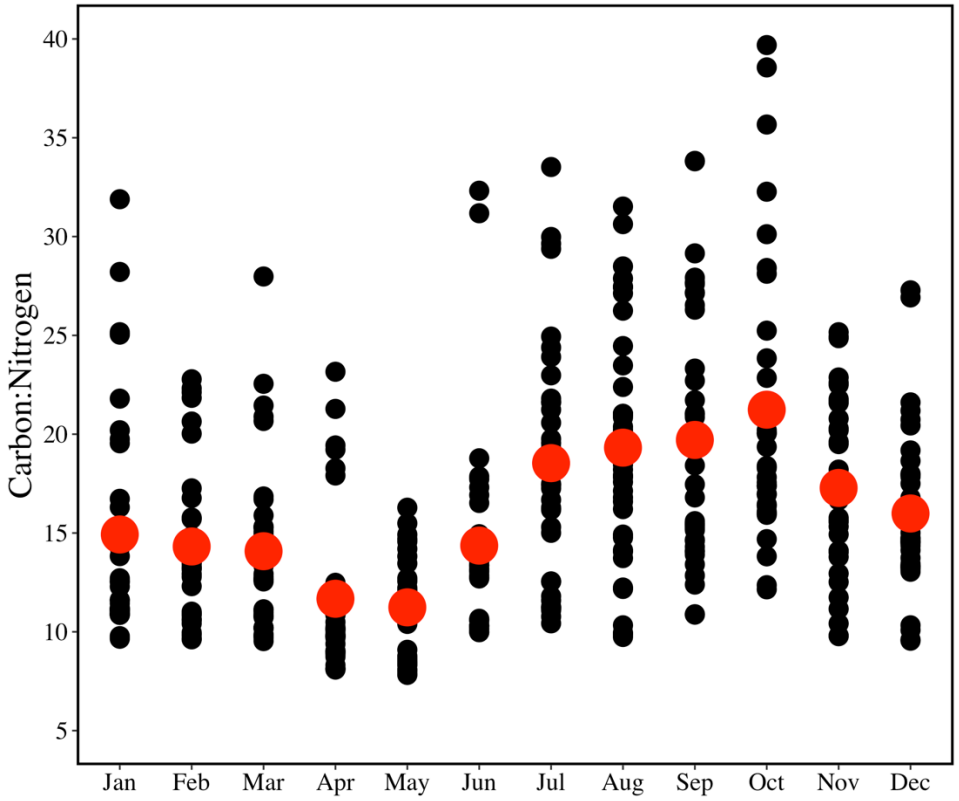

Supplemental Figure 5. Monthly giant kelp tissue carbon to nitrogen (grams: grams of kelp dry weight) sampled from Mohawk Reef between the years 2002 – 2021 (black circles). The large red dots are the monthly means over the time series record. Data was retrieved from the SBC-Long Term Ecological Research project (sbclter.msi.ucsb.edu/data/).

Supplemental Table 1. Summary statistics of the nine separate sampling and incubation events for the spring and summer cohorts including the date kelp was sampled for each incubation. Included are the mean ± 1 standard deviation of blade physiological measurements for the six replicate blades incubated at each time and the range of incubation light levels, rates of net primary production and net DOC exudation for the 18 rate measurements made per sampling event.

Season	Date	Age (d)	Blade C:N	Blade Chl:C	PAR (µmol m^{-2} s^{-2})	NPP (µmol C g_{DW}^{-1} hr^{-1})	DOC_{ex} (µmol C g_{DW}^{-1} hr^{-1})
Summer	8/9/23	16	29.9 ± 3.1	6.8 ± 1.7	0 - 1359	-24.6 – 264.9	-0.5 – 8.1
Summer	8/23/23	30	29.9 ± 1.5	6.4 ± 0.4	0 - 1517	-18.5 – 190.5	-1.2 – 5.9
Summer	9/5/23	43	29.1 ± 5.1	7.6 ± 2.2	0 - 1290	-19.2 – 159.0	0.0 - 6.7
Summer	9/26/23	64	34.8 ± 2.7	3.3 ± 2.1	0 - 1325	-23.4 – 93.9	1.9 - 44.5
Summer	10/10/23	78	35.7 ± 1.3	3.0 ± 0.9	0 - 1140	-30.3 – 61.0	2.8 - 65.3
Spring	4/17/24	16	9.8 ± 0.6	13.5 ± 4.4	0 - 1272	-23.7 – 195.6	0.2 - 6.6
Spring	5/7/24	37	10.4 ± 0.7	14.8 ± 3.4	0 - 1361	-25.0 – 172.0	0.2 – 6.0
Spring	5/28/24	58	9.9 ± 0.7	9.7 ± 2.8	0 - 1261	-28.8 – 153.2	0.2 - 27.7
Spring	6/16/24	77	15.2 ± 3.2	5.0 ± 2.5	0 - 1331	-28.0 – 117.0	1.4 - 35.2